

Moving graphs: Predicting barchan dune migration rates from their shapes

Daan Beelen

Utrecht University, Department of Physical Geography, Utrecht, the Netherlands

ABSTRACT

In this study, geometric perspectives on sand dune formation and motion are summarized, introduced, and combined to predict time-averaged velocities (migration rates) of barchan dunes directly from their shapes. First, it is proposed that smaller sediment accumulations outpace larger ones due to differences in surface-to-volume ratio. This ratio is defined by a bedform's wavelength and its wind-facing gradient, implying that relatively fast-moving, flat sediment volumes will be preferentially moved away to reveal slower-moving, tilted morphologies like ripple and dune-covered surfaces. Second, a power balance between wind shear and dune motion is used to show that dunes with a higher sediment flux tend to be steeper. As the size and steepness of dunes can be measured from satellite images, the aforementioned relationships can be combined to predict a barchan dune's speed directly from its geometry. The prediction is tested against satellite image time-series from nine active dunefields worldwide and is thereby shown to be universally accurate, making it the first successful prediction of its kind: $R^2 = 0.92$, $P = 2.0e-122$, $n = 250$.

In addition to understanding dune migration rates, this study also provides insights into the horned barchan and mirrored parabolic dune shapes, as well as the relationship between sediment flux and wind shear, supporting the splash-dominated model of particle entrainment.

[This manuscript is currently under review in the journal "Science Advances"]

Dunes are accumulations of sediment that migrate under the influence of a current. Their size and shape arise from interactions between the fluid and the sediment (Livingstone et al., 2007; Lancaster, 2023). Despite the complexity that arises from these interactions, there are simple geometric relationships related to dune sizes and shapes that, in some cases, capture the intricacy of sand dunes dynamics with remarkable accuracy (Howard et al., 1978).

In this study, the aim is to compile, combine, and deepen our geometric understanding of sand dunes and then use geometric relationships to make useful predictions that can be tested in nature. Specifically, a thorough analysis of the work of the seminal work of Bagnold, (1941), along with later concepts from Shehata et al. (1992), Momiji and Warren (2000), Andreotti et al. (2002), Melo et al., (2012), and Beelen (2021), suggest that barchan dune geometries may partially reflect their migration rate, but a direct derivation of a bedform's speed from its shape has never been achieved. This is unfortunate, as relating dune migration rates to their shapes can improve our ability to reconstruct ancient depositional environments (Eastwood et al., 2012) and enhance our understanding of environmental circumstances in inaccessible places like remote deserts, the deep ocean (Lonsdale and Malfait, 1974) or other planets and moons (Jerolmack et al., 2006; Jackson et al., 2015). To achieve this goal, an analytical solution for barchan dune migration rates and shapes is derived and is then used to predict the migration rates of sand dunes that have been measured from real-world, satellite image time-series of moving barchans. Barchan dunes are the main focus of this study because their size allows for accurate measurements of their geometry and migration rate from satellite images while their isolated arrangement ensures that their motion is not greatly affected by collisions and wind interference from nearby or amalgamated dunes. Barchan dunes can form and move for centuries across hundreds of kilometers of distance while maintaining remarkable consistency in their size and shape, enabling the measurement of long-term, steady state geometries (Long and Sharp, 1964; Haynes, 1989; Saurermann et al., 2000; Elbelrhiti et al., 2008). To isolate and emphasize geometric relationships, steady-state parameters are prioritized over time-dependent parameters that are often related to fluids like turbulence or short-term wind variability. Any such variable parameter considered in this study should therefore be regarded as a temporally and spatially averaged value (Lancaster, 2023, Chapter 4).

THEORY

List of abbreviations, parameters and their corresponding dimension:

Abbreviation	Parameter	Dimension
u_V	Dune migration rate	m/s
u_*	Wind shear velocity	m/s
u_s	Averaged velocity of the exposed sediment	m/s
z	Saltation layer thickness	m
A	Surface area exposed to the wind	m ² , m (2D)
V	Dune volume	m ³ , m ² (2D)
w	Dune width	m
λ	Dune length	m
h	Dune height	m
β	Angle of the wind-facing (stoss) side	-
α	Angle of repose	-
Q	Dune volume flux	m ³ /s, m ² /s (2D)
η	Wind efficiency (ratio of wind power converted into dune power)	-
C	Scaling parameter	s/m
ρ_s	Sediment density	kg/m ³
ρ_f	Air density	kg/m ³
g	Gravitational acceleration	m ² /s
P_s	Dune power	kg·m ² ·s ⁻³
P_f	Wind power	kg·m ² ·s ⁻³

Surface-to-volume ratios and sediment motion

A wind of sufficient strength will propel exposed sediment particles forward at an average velocity, herein denoted as ' u_s ' ^{Footnote 1}. Exposed sediment can be moved out of the way, in which case some previously buried material will become exposed. Sediment comprising a volume ' V ,' can thus cycle through phases of motion and burial so that it moves forward at an average speed ' u_V ,' determined by the rate of sediment motion multiplied by the fraction of exposed sediment (Beelen, 2021). Therefore:

$$u_V = u_s * \frac{V_{exp}}{V}$$

Buried sediment cannot be moved by the wind and only the uppermost layer of sediment is exposed, so the volume of moving sediment is equal to the exposed surface area ' A ' multiplied by the thickness of the saltation layer ' z ' so:

$$\text{Equation (1.1): } u_V = u_s * \frac{z * A}{V}$$

Across a uniform geometry, the surface-to-volume ratio: $\frac{A}{V}$ can be subdivided into infinitesimal wind-parallel cross sections. This is because the exposed surface area, as well as the sediment volume are both determined by the same factor of width:

$$\frac{A}{V} = \frac{A' * w}{V' * w} = \frac{A'}{V'}$$

The initial bed can be completely flat, in which case the exposed sediment is equal to the volume of the moving sediment. In this scenario, the ratio of exposed sediment to total sediment in the moving volume: $\frac{z * A'}{V'}$ is equal to 1, and the sediment volume will advance at its maximum rate of: $u_V = u_s$. In case the moving sediment volume is not flat, it is only partially exposed to the wind across height 'h,' a length facing the current (stoss side) 's,' and a length facing away from the current called 'lee' or, 'slip face' and has length 'l'. The sum of 'l' and 's' is the total length of the sediment volume parallel to the current direction (i.e. the wavelength), denoted as 'λ' (Fig. 1)

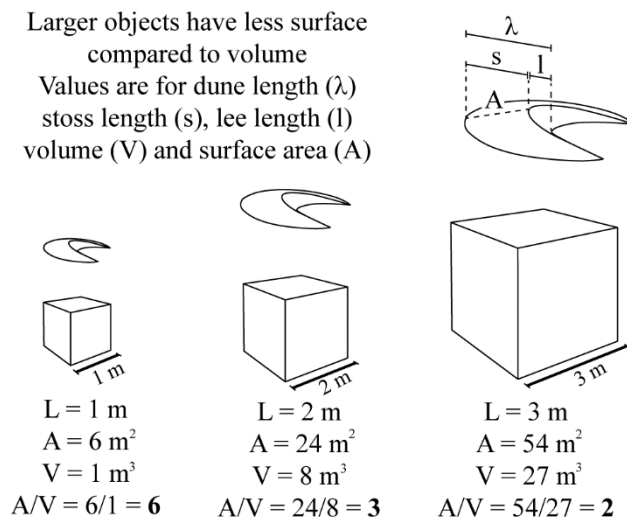


Figure 1. Schematic diagram illustrating the relationship between a cube's size and its surface-to-volume ratio. For a cube, the surface-to-volume ratio halves when the length doubles. The same principle applies to any object, with specific relationships varying based on shape. For sand dunes, the exposed surface area-to-volume ratio is determined by the size and the steepness of the stoss side.

Considering that any sediment volume, whether in motion or at rest, is inclined in both the lee and stoss directions, it can be approximated as a set of adjacent right triangles (Fig. 2). The sediment volume is therefore:

$$V' = \frac{1}{2} \lambda h$$

So the surface-to-volume ratio is:

$$\frac{A'}{V'} = \frac{A'}{\frac{1}{2} \lambda h} = \frac{2}{\lambda * \frac{h}{A'}}$$

Here, the exposed surface area A' can be approximated as the hypotenuse of the height and the stoss side length (Fig. 1, ^{Footnote 2}). The surface-to-volume ratio can thus be redefined in terms of the length of the moving sediment volume and the gradient of the windward stoss side (Fig. 2; Angle β):

$$\text{Equation (1.2): } u_v = \frac{2u_s z}{\lambda * \sin \beta}$$

From equation (1.2) it is clear that the migration rate of any sediment volume is inversely proportional to its size (herein characterized by λ ; see Fig. 1) and the steepness of the current-facing stoss side (β). As sediment is moved by a current, the relatively fast-moving, untitled bed will be deflated to reveal a slower and therefore more stable tilted morphology covered by ripples and/or dunes (Fig. 2). Realistically, a perfectly flat bed will inevitably become uneven as the rapidly moving, flat material is preferentially moved away to reveal more stable, tilted bedforms. This process is analogous to a riverbed that is covered by coarse-grained gravel, lacking the faster-moving sand and clay that has been preferentially moved by the current. Since width cancels out in the surface-to-volume ratio, a sediment-covered surface will generate parallel ridges that migrate uniformly in the direction perpendicular to the wind direction. Any current environment with moving sediment will, therefore, develop towards: $\beta > 0$. Ripples, whereby λ is equal to the average length of a saltation hop (Bagnold, 1941), are likely to be the most common bedform but any value for λ or even multiple values for λ (i.e. superimposed or, compound

bedforms) are possible. In most cases, trains of fluid instabilities, characterized by one or more environment-specific modes, will determine λ (Kennedy, 1969).

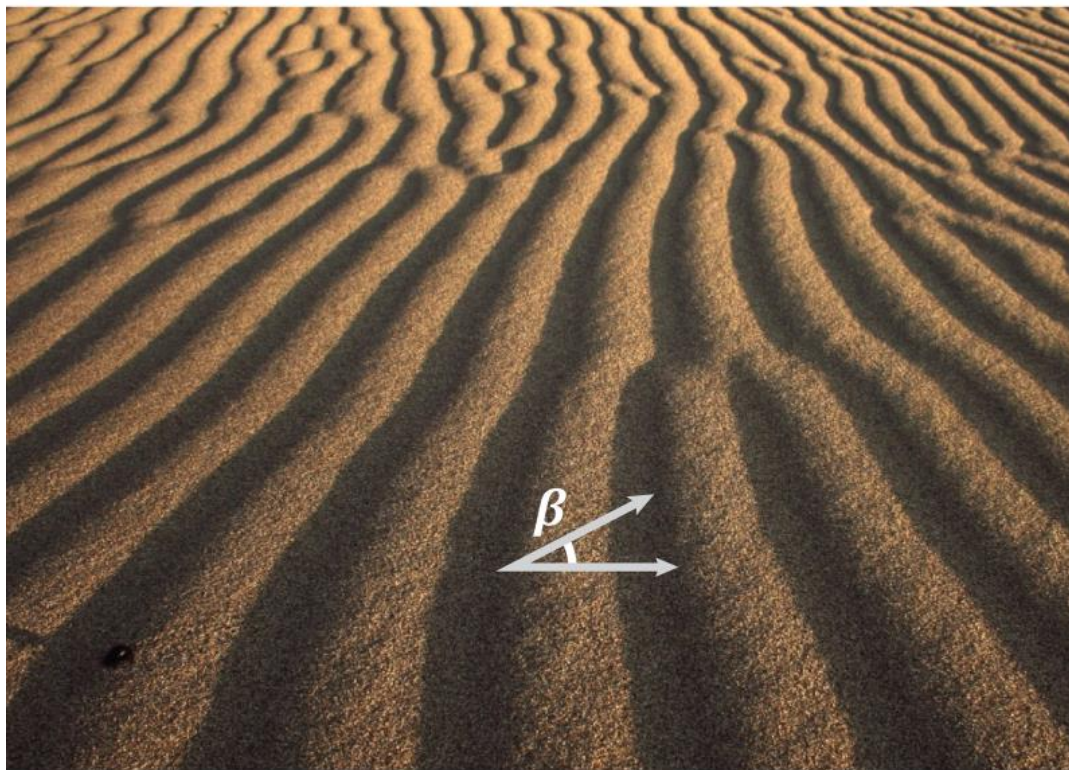
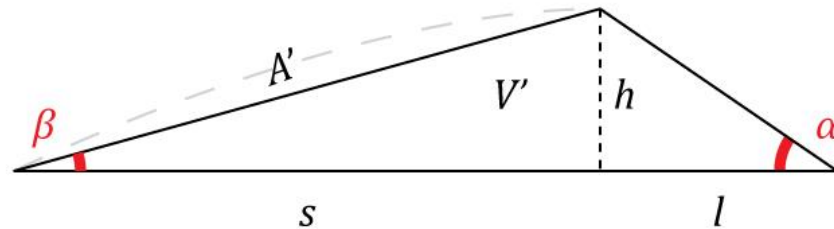


Figure 2: Illustration of a sand dune in the wind-parallel cross-section. The stoss side has a base denoted as 's' and height as 'h' with a sharp angle ' β '. The lee triangle has a base 'l' and height 'h' with a sharp angle equal to the angle of repose: ' α '. Although the dune width is not illustrated in the diagram, it is represented by 'w'. The diagram is accompanied by a photograph of a rippled surface showing the geomorphology of a sand-covered bed that has $\beta > 0$.

Explaining barchan dune shapes

In case a sediment volume is laterally limited in size like an isolated parcel of sediment or 'protodune' (Baddock et al., 2018; Qian et al., 2021), the parcel's fringes are smaller and thus have higher surface-to-volume ratio and migration rate compared to its center. This causes the fringes to outpace the center and develop a 'horned' shape that is characteristic for barchan dunes (Fig. 3A). Moving from the center to the fringe, each subsequent segment increases in surface-to-volume ratio in across a parabolic trend with the fringes outpacing the center as a function of the dune's width. This parabolic relationship between migration rate and width is results in a barchan's parabola-shaped horns (Fig. 3A).

Now consider the same sediment volume but dissected horizontally. Higher segments are smaller so the surface-to-volume increases towards the top, resulting in a parabola-shaped, stoss side. This increase in migration rate from bottom to top will cause the sediment to oversteepen on the forward facing lee face (Sutton et al., 2013; Fig. 3B). The oversteepening sediment will eventually cascade down the lee face that initially forms at the base and develops upwards (Elbelrhiti, 2012). Sediment sitting on the lee face will cascade downwards under gravity and is not directly affected by the dominant wind, so the lee face angle α is equal to the angle of repose (Pye and Tsoar, 2008; angle α ; Fig. 3C). Bagnold (1941), Chapter 13, provides an analogous analysis on the increase in sediment motion towards the top of the dune and the formation of a lee face based on geometric considerations.

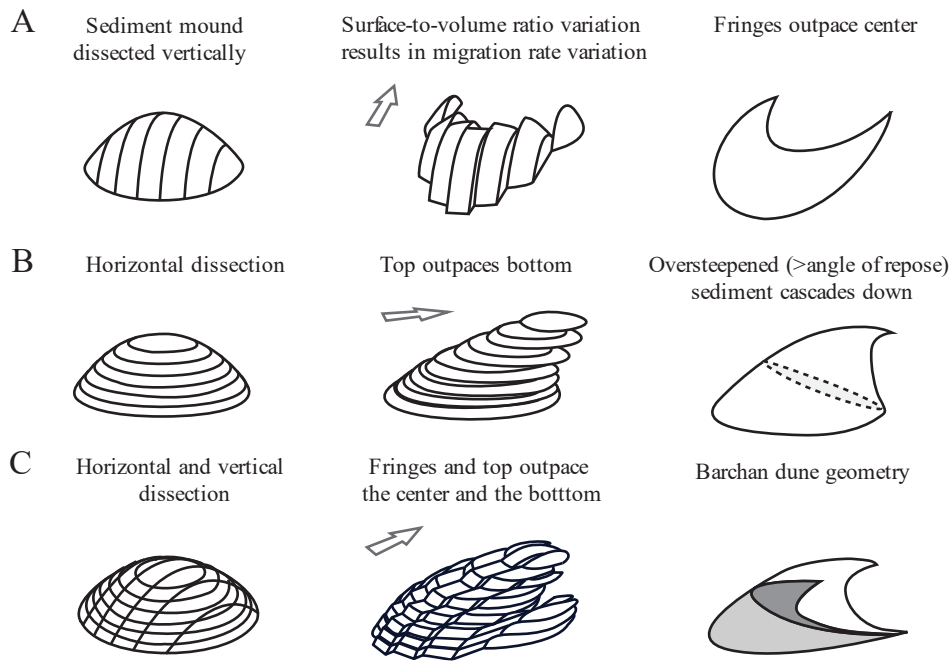


Figure 3. Variation in surface-to-volume ratio explains barchan dune geometry. A. Consider a sediment mound that is dissected perpendicular to the wind direction. In this illustration, the mound is dissected into seven volumes. The volumes at the fringes have a higher surface-to-volume ratio and correspondingly, higher migration rate. This implies that the fringes outpace the center leading to the characteristic 'horned' barchan dune shape. B. Dissections across the vertical imply a relatively fast top, leading to a parabolic stoss side and oversteepening with associated sediment cascading down the forward lee face. C. Dissections in both dimensions result in a complete barchan dune equilibrium shape with a parabolic stoss side, a diagonal lee face and a 'horned' footprint geometry. The arrow shows the dominant wind direction and direction of dune migration.

Dune volume flux

A sand dune's volume flux can be easily derived from graphical considerations of a 2D dune profile. Consider that the dune's volume flux is equal to the surface area of the parallelogram $h*d$, where 'd' is the dune's displacement across an increment of time (Bagnold, 1941). Therefore:

$$Q' = u_v h$$

This relationship dictates that under uniform conditions of dune volume flux, like amongst dunes that are migrating within the same dunefield, dune migration rates must be inversely proportional to their height. Since inverse height has the same dimension as surface-to-volume ratio (m^{-1}), it follows that these concepts may be consistent. The geometric relationship between dune volume flux and height can therefore be combined with the relationship between migration rate and 2D surface-to-volume ratio, resulting in an equation that relates the volume flux with the shape of the dune. To show this, consider again equation (1.1):

$$u_s z = u_v * \frac{V'}{A'} = \frac{1}{2} u_v h * \frac{\lambda}{A'}$$

This is equal to:

$$2u_s z = Q' * \frac{\lambda}{A'}$$

Consider:

$$\frac{\lambda}{A'} = \frac{l + s}{A'} = \frac{l}{A'} + \frac{s}{A'}$$

This term can be rewritten as a trigonometric function:

$$\frac{l}{A'} + \frac{s}{A'} = \frac{\sin \beta}{\tan \alpha} + \cos \beta$$

Inversely:

$$\left(\frac{\sin \beta}{\tan \alpha} + \cos \beta \right)^{-1} = \frac{\sin \alpha}{\sin(\alpha + \beta)}$$

The volume flux of the dune can be expressed in terms relating to the dune's shape:

$$\text{Equation (2): } Q' = 2u_s z * \frac{\sin \alpha}{\sin(\alpha + \beta)}$$

Equation (2) highlights that the volume flux of a sand dune can differ significantly from the bedload flux across dune's stoss side, which is proportional to u_s (Valence et al., 2015; Durán et al., 2012). This is an important notion that is not always adequately considered in derivations of sediment flux and current velocity.

Wind power

To further investigate how the aforementioned geometric principles can be used to link dune migration rates with their shapes we can construct a power balance between the wind power and the mechanical power of the dune. Since all the power of the dune comes from the wind we can state that:

$$P_f = P_s * \eta$$

Here, ' η ' is the efficiency, i.e. ratio of wind power converted into mechanical dune power. The wind power across the dune ' P_f ' can be defined as the kinetic energy of the wind that passes over the dune per increment of time. The mass of air that is moved across the dune depends on air density ' ρ_f ' as well as the dune's width and height. It is also determined by the windspeed, which sets the length of the parcel of air that moves across the dune within the increment of time considered. The wind power is therefore defined as air density multiplied by width, times height, times wind speed cubed (i.e. the 'wind turbine equation'; i.e. Manyonge et al., 2012):

$$P_f = \frac{1}{2}hw * u_*^3 * \rho_f$$

In this context, we are considering only the wind that drives the motion of the sand dune in a time-averaged sense, which means that directional variability of the wind as well as periods where the wind is not strong enough to move any sediment are not included. This 'effective wind speed' refers to the velocity component of the wind that is moving the sediment, whereby the threshold of motion and any friction are not considered. The effective wind speed is also vertically homogeneous and must therefore be described as a friction or, shear velocity (Pye and Tsoar, 2008, Chapter 2). Note that barchan dunefields are mostly devoid of vegetation and sand dunes tend to be taller than 1 m so the boundary layer effects that occur close to the bed likely do not play a significant role (Pye and Tsoar, 2008; Kok et al., 2012). To express the mechanical power of the moving dune ' P_s ', consider that the dune sits above the surface, having a gravitational potential energy dependent on its height and sediment mass density. Sediment cascades downward from the dune's summit in an amount that is

proportional to its volume flux ' Q '. The dune's mechanical power can therefore be expressed as the height squared multiplied by its speed of motion, as well as dune's width, its sediment density and the gravitational acceleration:

$$P_s = h^2 w * u_v * g \rho_s$$

Expanding the power balance:

$$\frac{1}{2} h w * u_*^3 * \rho_f = h^2 w * u_v * \eta * g \rho_s$$

Width cancels out again and a factor of height also cancels out therefore:

$$u_*^3 = Q' * \eta * 2g \frac{\rho_s}{\rho_f}$$

From geometric principles it thus follows that the dune's volume flux is proportional to the effective wind shear cubed. We can gain further insight into this equation by expressing the efficiency factor ' η ' in terms of the dune's geometry. Consider a dune with a stoss side that is twice as long as its lee face. In case of an optimal efficiency, $\eta = 1$, sediment mass balance necessitates that all of the moving sediment across the stoss side ends up on the lee face. Therefore, every grainsize diameter length ' φ ' of advance of the longer stoss side, must coincide with a 2φ advance on the shorter lee face. This results a difference in the speed of advance between the back and the front of the dune which would cause the dune to become less steep over time and eventually disappear. The steady-state dunes considered in this study remain constant in shape throughout migration, so we must conclude that only half of the sediment climbing up and over the aforementioned hypothetical stoss side can cascade down the lee face. The other half of the moving sediment must be lost either from the brink of the dune or laterally towards the barchan's horns (Hersen, 2004; Durán et al., 2010). This lost sediment was elevated by wind power but is lost from the dune's volume so it did not contribute to the mechanical power of the dune's motion. The fraction of wind power converted into mechanical dune power is therefore proportional to the ratio of the stoss side hypotenuse length versus lee face hypotenuse length which is:

$$\eta = \frac{A'_{lee}}{A'} = \frac{\left(\frac{h}{\sin \alpha}\right)}{\left(\frac{h}{\sin \beta}\right)} = \frac{\sin \beta}{\sin \alpha}$$

Therefore:

$$\text{Equation (3.1): } u_*^3 = Q' * \frac{\sin \beta}{\sin \alpha} * 2g \frac{\rho_s}{\rho_f}$$

Equation (2) can be substituted into equation (3.1) to determine the relationship between wind shear and dune shape:

$$u_*^3 = 2u_{sz} * \frac{\sin \alpha}{\sin(\alpha + \beta)} * \frac{\sin \beta}{\sin \alpha} * 2g \frac{\rho_s}{\rho_f}$$

Which is:

$$\text{Equation (3.2): } u_*^3 = u_{sz} * \frac{\sin \beta}{\sin(\alpha + \beta)} * 4g \frac{\rho_s}{\rho_f}$$

Wind shear and sediment flux

Equation (3.2) contains both the wind shear and the average sediment speed, which are inevitably related. We can therefore explore this relationship even further and derive the relationship between the wind shear and the dune's shape. To achieve this, it is not sufficient to rely on the dune's geometry alone so we have to consider the physical relationship between wind shear and sediment entrainment. Fortunately, there have been many studies that have sought to derive and experimentally understand such relationships, e.g., Bagnold, (1941); Ungar and Haff, (1987); Andreotti, (2004); Valence et al., (2015). Most recent studies suggest that wind shear has no direct relationship with the speed of the entrained, moving sediment, but the proportion of sediment grains that is moving is linearly proportional to shear stress and quadratically proportional to the wind shear ($u_s \sim u_*^2$, Martin and Kok, 2018). Since we are considering the effective wind shear, the velocity at the threshold of motion can be ignored. It can therefore be stated that:

$$u_s = C * u_*^2$$

Here, 'C' is a scaling parameter that is introduced to account for various factors that influence the wind-driven motion of sand grains. It should also be acknowledged that this statement is

greatly simplified and that numerous interpretations exist regarding the relationship between sediment motion and wind shear. Because in this study the analysis is concentrated on dune geometry, it may be sufficient for now, to simply consider the appropriate proportionality while passing by other aspects like particle hop time and variable saltation heights, which also have an effect. This simplification enables us to validate the geometric theories, without delving deeply into other sedimentary dynamics. See Valence et al. (2005); Andreotti (2004); Dong et al. (2003); Sørensen (2004); Kok et al., (2012); Martin and Kok, (2018) for much more in-depth analyses on the physical relationship between eolian sediment transport and wind shear.

Substituting the aforementioned term into equation (3.2) yields an expression that relates the wind shear to the dune's shape:

$$\text{Equation (4.1): } u_* = \frac{\sin \beta}{\sin(\alpha + \beta)} * zC4g \frac{\rho_s}{\rho_f}$$

Since everything other than 'u*' and 'β' generally remains constant for any barchan dune, the stoss gradient 'β' should go up with increasing wind shear. This notion, that higher wind shear leads to steeper dunes, is supported by Howard et al. (1978).

Equations (3.1) and (4.1) can be combined to estimate a barchan dune's volume flux from its shape:

$$\sqrt[3]{Q' * \frac{\sin \beta}{\sin \alpha} * 2g \frac{\rho_s}{\rho_f}} = \frac{\sin \beta}{\sin(\alpha + \beta)} * zC4g \frac{\rho_s}{\rho_f}$$

So:

$$Q' = \frac{\frac{\sin \beta}{\sin(\alpha + \beta)} * zC4g \frac{\rho_s}{\rho_f}^3}{\frac{\sin \beta}{\sin \alpha} * 2g \frac{\rho_s}{\rho_f}}$$

Which is:

$$\text{Equation (4.2): } Q' = \frac{\sin \alpha \sin^2 \beta}{\sin^3(\alpha + \beta)} * 32z^3 C^3 * g \frac{\rho_s^2}{\rho_f}$$

According to equation (4.2), a measurement of a dune's shape can be used to predict its volume flux. This prediction can be combined with measurements of the dune's size to predict the dune's migration rate.

VALIDATION

To validate the theory, time series of actively migrating dunes are obtained from Landsat satellite images. These images are georeferenced and time-stamped, so the sizes and migration rates of dunes can be recorded and plotted, in a similar way to previous studies like in Michel et al. (2018), Baird et al. (2019) and Zheng et al. (2022). For each dunefield considered, a rectangular sampling perimeter is outlined, and all stoss side lengths (s) and lee face lengths (l) are measured. Dune displacement between timesteps are also measured to calculate their migration rates. Timesteps between sequential satellite images are always several years (2-32 years) long, to accommodate seasonal changes in wind patterns and migration rates (Bristow, 2019). All measurements are in the supplementary information (S1).

Linear relationship between migration rate and surface-to-volume ratio

Measurements confirm that for nearby dunes, migration rates correlate linearly to their surface-to-volume ratios (Fig. 4). Furthermore, the inverse of any other one-dimensional parameter (such as length, width, height, etc.), correlates linearly with migration rate. Accordingly, the square root of two-dimensional surface area, is inversely proportional to migration rate.

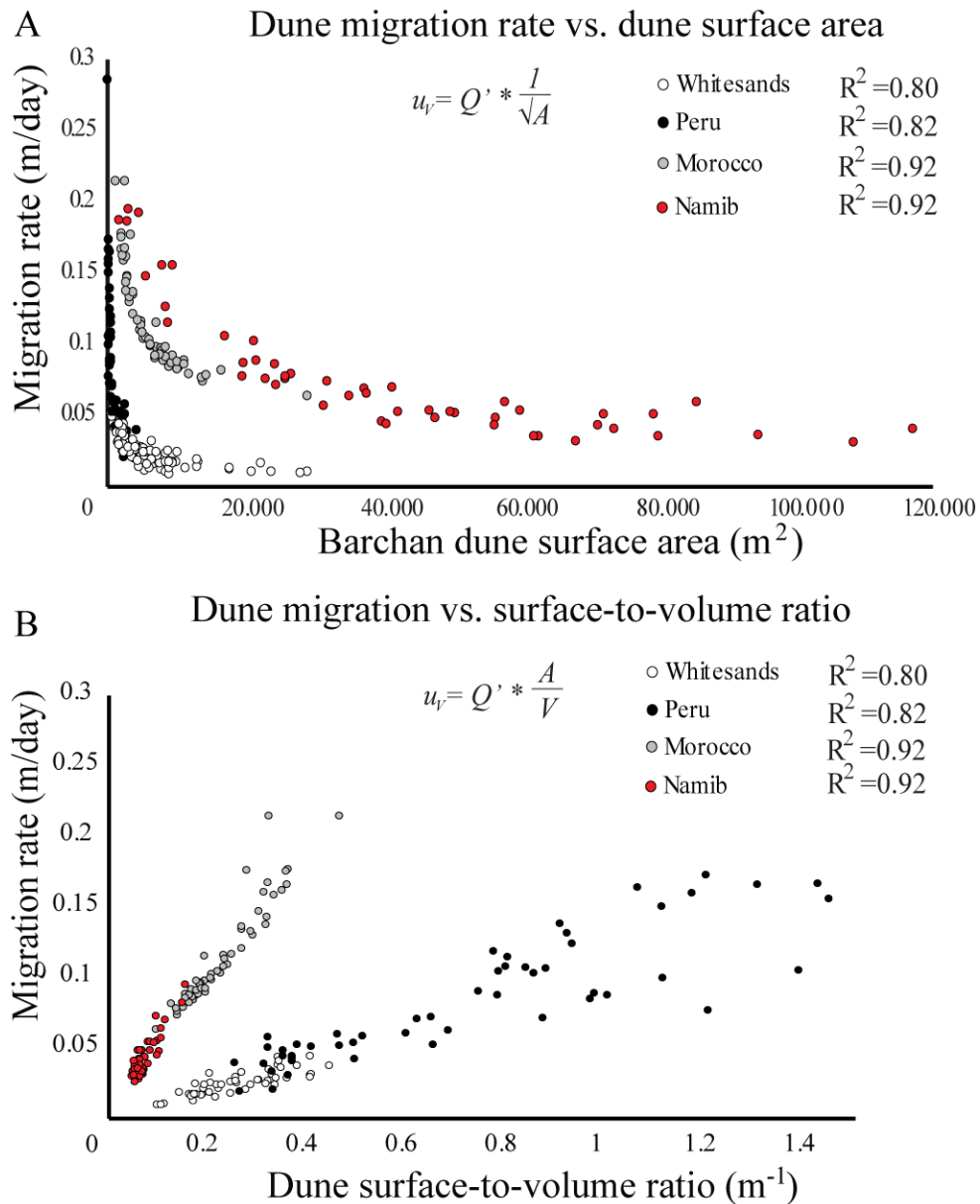


Figure 4. A. Graph showing dune migration rate versus footprint surface area measured from satellite images of moving barchan dunes. Each data point represents one dune, each color represents a dunefield. B. The same data as in A. but now the surface-to-volume ratio has been calculated from measurements of stoss side and lee face length (see figure 1). Within each dunefield, surface-to-volume ratios are linearly correlated to migration rates.

The velocity of the exposed sediment u_v can be obtained by measuring the speed of the dune and the surface-to-volume ratio (Equation 1.1) and assuming a saltation cloud thickness that is constant for different windspeeds (Martin and Kok, 2017). Measured sediment velocity is found to be roughly the same and normally distributed within each dunefield but it varies by as much as twenty times from one dunefield to another ^{Footnote 3}.

Dimensional analysis shows that a dune's volume flux reflects a surface area covered by a dune per unit of time. This is corroborated by measurements, which indicate that dunes under similar environmental conditions, within the same dunefield, cover roughly the same surface area per unit of time, regardless of their size (see supplementary information; S2). In essence, small dunes cover a long, narrow surface area equal to that of an adjacent, larger dune's short and wide covered area (Fig. 5; Andreotti et al., 2002). This demonstrates that measurements under natural conditions are dimensionally consistent with the theory.

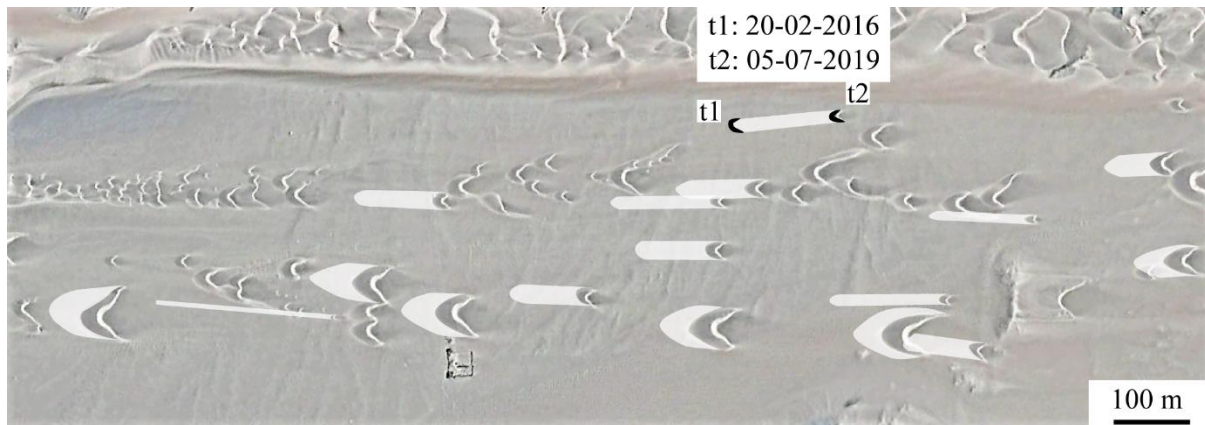


Figure 5. Satellite image showing that dune volume fluxes are consistent across dunefields. Image shows migrating barchan dunes in Ancash, Peru: 9°20'02"S, 78°20'56"W. Surface areas covered between t1 and t2 are highlighted as grey polygons. In this area, dunes cover $2.1 \pm 1.0 \text{ m}^2/\text{day}$ which is irrespective of dune size and speed. Surface area covered is equivalent to the dune volume flux.

Parabolic dunes

An essential aspect of the theories presented in this work is that the surface-to-volume ratio variability across a dune's shape defines its geometry (Fig. 3). Robust evidence supporting this notion comes from comparing barchan dunes with parabolic dunes. The latter dune type typically forms in areas where the water table is closer to the surface. Such conditions cause vegetation to fixate the sediment into place, making parabolic dunes very slow (Reitz et al., 2010). Parabolic dunes are governed by different dynamics than barchan dunes because their surface areas do not promote their motion (Barchyn et al., 2012). Larger vegetated surface areas further inhibit sediment motion for dunes of this type. A suitable area to compare these dynamics is the Whitesands dunefield in New Mexico, USA, where actively migrating barchan dunes and parabolic dunes exist in close proximity (Reitz et al., 2010).

Measurements of both dune types were made following the methodology explained

previously, and the results are graphed side-by-side in Figure 6. This reveals that for parabolic dunes, equation (1.1) is inverted, with larger parabolic dunes moving faster than smaller ones. Earlier, it was proposed that for barchan dunes, a higher surface-to-volume ratio at the fringes makes them outpace the center, generating the forward-facing ‘horned’ equilibrium geometry. When the relationship between surface-to-volume ratio and migration is reversed like with parabolic dunes, we instead find that, the center outpaces the fringes which causes the dune’s horns to point backward. As a result, the planform geometries of parabolic dunes are mirrored when compared to barchans. The same effect is also apparent from measurements of the vertical cross-section, which is concave for barchans (Figs. 3; 6C), but convex (hollow) for parabolic dunes (Fig. 6C). The mirrored cross-sectional geometry of parabolic dunes supports the notion that variability in surface-to-volume ratio defines the dune’s shape and thereby contradicts the theory that dune shape is determined by streamlines across the stoss side (i.e. Wiggs et al., 1996). The inverted relationship between size and migration rate for parabolic dunes can be observed in any parabolic dunefield, such as at Great Sand Dunes, CO, USA (37°41’N, 105°35’W), or in Ash Sharqiyah, Saudi Arabia (25°55’N, 49°58’O), as shown in supplementary information (S3).

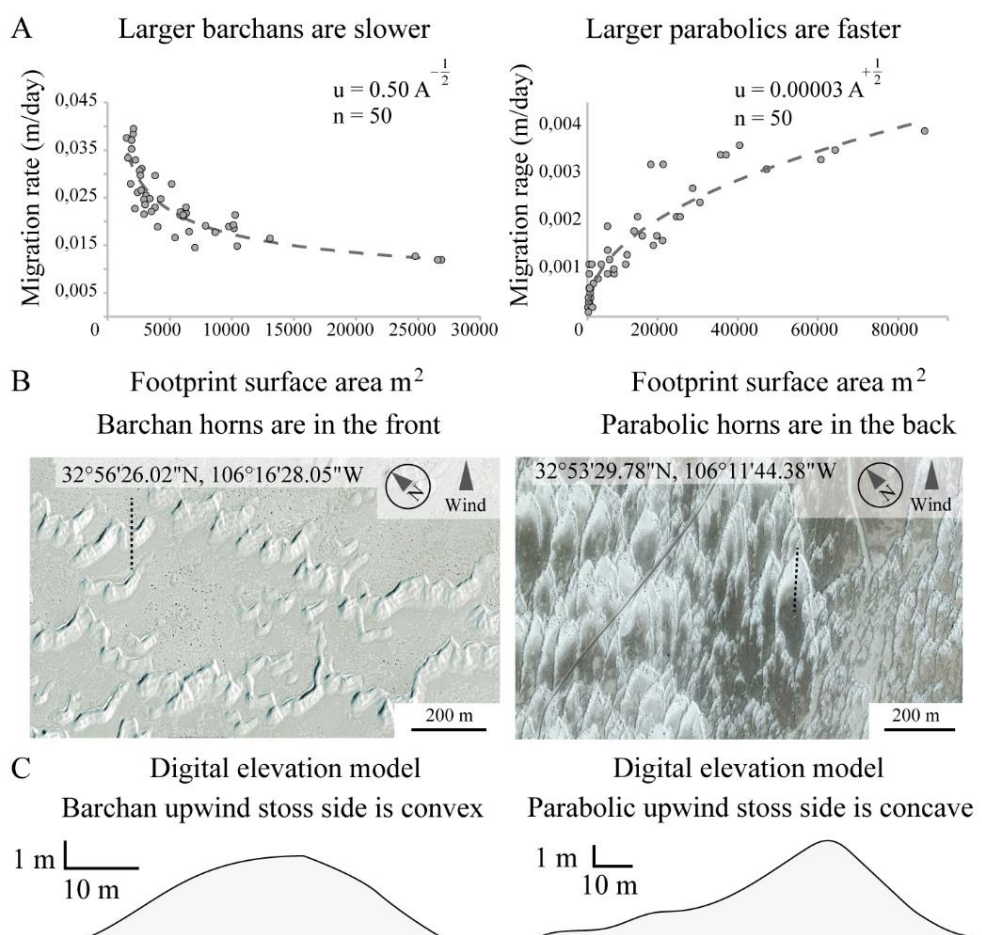


Figure 6:A: Graphs illustrating the relationship between surface area and migration rate for barchan dunes (left) and parabolic dunes (right) in the same dunefield (Whitesands, NM, USA). Note the mirrored relationship between these two. B: Satellite images of barchan dunes and parabolic dunes in Whitesands. C: Vertically exaggerated topographic cross-sections of a barchan dune and a parabolic dune in Whitesands. The location of the cross-section is indicated by the dotted line in (B). A 30-cm vertical resolution DEM from LiDAR data is available in Ewing et al. (2012). Note that in planform and in cross-section the geometries of these dune types are mirrored, reflecting the mirrored relationship shown in (A), according to the principle shown in Figure 3.

We can now test the proposed relationship between surface-to-volume ratio and geometry by comparing barchan dunes under various environmental conditions. Very low sediment fluxes can be measured on Mars (Chojnacki et al., 2017), and in accordance with equation (3.1), these barchan dunes exhibit a very low-angle stoss side (Fig. 7) ^{Footnote 4}. On Earth, barchan dunes migrate in more energetic wind conditions, displaying a steeper stoss side geometry

(Fig. 7). Overall, the measurements reveal a universal, positive correlation between dune volume flux and stoss side gradient (Fig. 8A). Higher stoss side gradients also consistently correlate with lower aspect ratios (proportionately wider dunes). In essence, a barchan dune can be regarded as a naturally-occurring graph that visually represents its volume flux through its stoss side gradient and aspect ratio. As predicted by equation (4.1), this concept can be extrapolated across vastly different regions and environments, suggesting that there is a universal relationship between a dune's geometry and its environment.











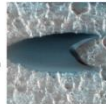

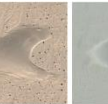

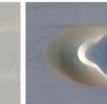
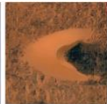
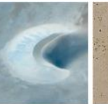



	Mars	Whitesands	Taklamakan	Peru	Yemen	Egypt	Chad	Libya	Morocco	Namib
	18°14'5"N 100°15'1"O	32°58'6"N, 106°22'3"W	36°58'2"N, 82°35'3"E	09°15'5"S, 078°17'5"W	14° 3'1"N, 47°49'4"O	24°55'0"N, 030°28'4"E	19°20'2"N, 020°17'3"E	24°24'0"N, 018°27'5"E	27°16'1"N, 013° 11'2"W	26°53'3"S, 015°18'6"E
Q' (m ² /day)	0.03	0.06	0.08	0.15	0.32	0.32	0.43	0.52	0.92	1.42
β (deg.)	3.4	3.2	3.9	5.2	6.4	6.0	6.3	7.5	9.6	13.4
Shape										
Image (not to scale)										

Figure 7: A compilation of averaged dune volume fluxes (Q') and stoss side angles (β) in various dunefields. Each measurement is accompanied by a satellite photo and a geometric outline of a representative dune within that dunefield. Note that stoss side angle universally increases with dune volume flux which is predicted by equation (4.2).

Predicting migration rates from dune geometries

We have determined that steeper dunes have a higher volume flux. To predict migration rates, we can calculate stoss side gradients from lee face (l) and stoss side lengths (s).

Consider:

$$h = \frac{l}{\tan \alpha}$$

So:

$$\beta = \tan^{-1} \left(\frac{l}{s \tan \alpha} \right)$$

Other factors like the angle of repose for sand and sediment and fluid densities are roughly constant for each dunefield so we can use some following representative values for the prediction (Sutton et al., 2013; Martin and Kok, 2017; Lancaster, 2023):

Abbreviation	Parameter	Value	unit
z	Saltation layer thickness	0.05	m
ρ_s	Sediment density	1442	kg/m ³
ρ_f	Air density	1.290	kg/m ³
g	Gravitational acceleration	9.81	m ² /s
α	Angle of repose	34	degrees

Dune volume fluxes can be predicted using these values and equation (4.2). Since: $Q' = u_v * h$, we can divide the predicted fluxes by the height of each dune to obtain its migration rate. This prediction is statistically significant, $R^2 = 0.6$ but there are two problems that should be accounted for to make the prediction more accurate. The first problem is that the dune's height partially sets the stoss side gradient so by dividing $\sin \beta$ by h , the sediment flux prediction becomes distorted. As mentioned earlier, any one-dimensional parameter can be used to characterize a dune's size, so a measure that is less closely related to the stoss side slope while still encompassing the dune's size like the length ' λ ' should instead be used to mitigate the distortion. Secondly, measured migration rates are time-averaged while the migration rate predictions are from a single image and represent a single moment in time. Owing to equation (1.1), the geometries of smaller dunes will be affected more by transient changes in the wind. As the wind is never totally constant on short timescales, dune slopes at any given moment will be slightly different between dunes of different size, even when the wind is spatially constant across the dunefield. To correct for this, sediment fluxes can be predicted from stoss side angles that are averaged across a dunefield. Taking the aforementioned into account, the following predictor for a dune's migration rate from its shape is derived:

$$u_v = \frac{\overline{\sin \alpha \sin^2 \beta}}{\sin^3(\alpha + \beta)} * 32C^3 z^3 * g \frac{\rho_s^2}{\rho_f} * \lambda^{-1}$$

The best fit with measured migration rates shows that $C \approx 0.0002$ s/m. Predictions from this methodology resulted in the values shown in Fig. 8B and C which correspond well to

measured migration rates ($R^2 = 0.96$, $P = 2.0e-122$, $n = 250$; see supplementary information; S4, S5).

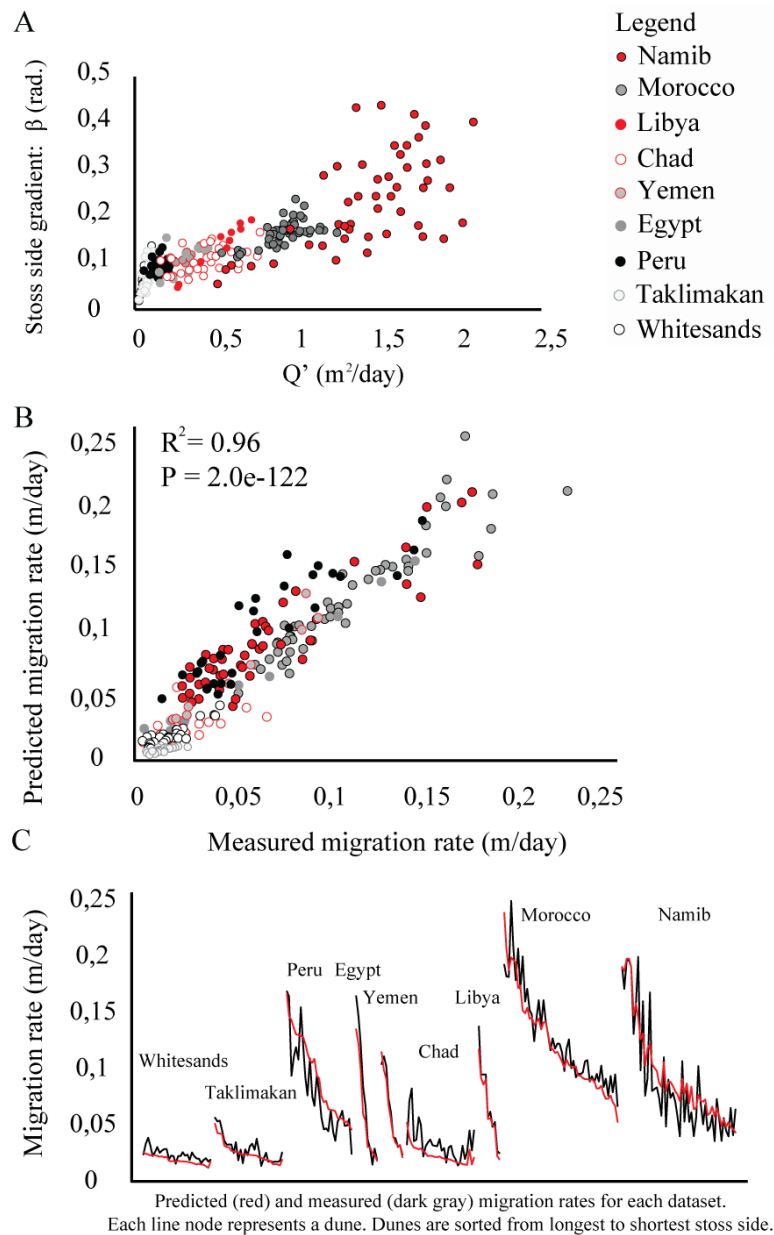


Figure 8: A. Graph showing the regression of sediment flux (Q') and stoss side gradient, illustrating their universal correlation across different dunefields as predicted by equation (4.2). B. Regression analysis indicating that measurements of stoss side angle and length can predict migration rate. C. The same data as in B but presented in a different graph format, showing predicted (dark grey) and measured (red) migration rates for each dataset. Each line node represents a dune, sorted from longest to shortest stoss side. Predictions are accurate across a wide range of dunes and dunefields and assume the same values for angle

of repose, saltation layer thickness, sediment density, air density and gravitational acceleration.

DISCUSSION

The predictions appears to be more accurate in dunefields with relatively large, stable dunes like Namib or Morocco as opposed to dunefields with more variable, small dunes like in Peru. This is probably because the steady state geometries of dune movements are easier to capture in less dynamic environments. Small and relatively fast dunes like in Peru collide and merge more often than larger dunes, which also necessitates the use of shorter timesteps in such dynamic dunefields. This also has the effect of averaging out less random noise which increases the amount of randomness.

The surface-to-volume ratio principle in combination with other previously mentioned geometric principles explain many of the observed bedform dynamics as well as a simple explanation for the origin of ripples and sand dunes without the need to invoke the fluid instabilities. Although no theory on dune formation and motion is complete without proper consideration of fluids, it is important to reflect on the invariable formation of barchan dunes in laboratory settings (Hersen et al., 2002) and widely diverse natural environments, ranging from deserts to the deep ocean (Lonsdale and Malfait, 1974). This consistent occurrence across disparate settings may support the notion that geometric properties, which are universal across every scale and fluid medium, dominate the origin and formation of sand dunes. Although further work is necessary to expand the equations derived here to other bedform types like laterally continuous ripples and transverse dunes and other fluid regimes like subaqueous settings.

The geometric perspectives outlined herein may also be consistent with the bedform stability paradigm. To explain this, consider that the limit to equation (3.2) which is met when stoss side steepness matches the angle of the repose. In this case, the sediment on the stoss side will become oversteepened and cascade down, eroding the sand dune. The geometric relationship between dune shape and wind shear therefore predict that there is a maximum stoss side slope which is: $\beta = \alpha$ which is consistent with the fact that under high current velocity conditions, bedform stability fields will change, eroding ripples or dunes (i.e. 'plane bed', Southard, 1991). From the data collected here, it can be estimated that the upper limit for barchan dune sediment flux migration rate is: $Q'_{max} \approx 1.5 \text{ m}^2/\text{day}$ which is near the limit of the observed sand dunes of the Namib dunefield. In addition to geometric relationships, the data collected in this study also gives insights into the

saltation and entrainment behavior of sand grains (Melo et al., 2012; Pähtz and Durán, 2017). It can be assumed that taller dunes are exposed to higher averaged wind speeds due to the logarithmic boundary layer profile. If wind speed is related to sediment flux, the implication is that taller dunes within the same dunefield must have a higher sediment fluxes, as was anticipated by Bagnold (1941). To test this assumption, we can relate dune sediment flux with height within each dunefield. This hypothesis can be described as: $Q' \sim h$. The test yields a poor correlation in every dunefield ($0.01 < R^2 < 0.3$) implying that under uniform conditions of wind shear, taller dunes do not have significantly more sediment flux, despite being exposed to higher wind speeds. The prevailing explanation for this is that sediment motion is dominantly facilitated by impacting sand grains, which become less abundant, higher up in the boundary layer (Melo et al., 2012). The decrease in grain impacts with height must therefore negate the increase in wind speed as a driver of sediment motion, supporting the ‘splash-dominated’ entrainment model for natural conditions, a model that is corroborated by previous studies (Pähtz and Durán, 2017; Martin and Kok, 2017).

FOOTNOTES

Footnote 1: ‘ u_s ’ represents the average velocity of all exposed sediment particles on the bed and within the saltation layer. It includes exposed particles that are not moving and thus have a speed of 0. u_s is therefore different from, for example, the horizontal particle velocity ‘ V ’ (Martin and Kok, 2017) which is the average speed moving (entrained) particles which have a speed >0 . In order to obtain the saltation flux, V must be multiplied by the saltation particle concentration ϕ . Experiments show that V does not change much with increasing u^* but ϕ , does scale quadratically with u^* . As u_s is directly proportional to ϕ , it is analogous to the saltation flux which scales quadratically with u^* (Martin and Kok, 2017).

Footnote 2: The stoss side is not diagonal but parabolic; however, this simplification does not affect the overall concept. The value for the stoss side angle represents the average gradient of the parabolic stoss side.

Footnote 3: Sediment fluxes do not significantly deviate from a reference standard deviation. See the Kolmogorov–Smirnov normality test in the supplementary information (S7).

Footnote 4: Data from the Martian barchans are sourced from the HiRISE orbiter and published in Chojnacki et al. (2020).

REFERENCES

- Livingstone, I., Wiggs, G. F., & Weaver, C. M. (2007). Geomorphology of desert sand dunes: A review of recent progress. *Earth-science reviews*, 80(3-4), 239-257.
- Lancaster N. *Geomorphology of Desert Dunes*. 2nd ed. Cambridge University Press; 2023.
- Howard, A. D., Morton, J. B., GAD-EL-HAK, & Pierce, D. B. (1978). Sand transport model of barchan dune equilibrium. *Sedimentology*, 25(3), 307-338.
- Bagnold, R. A. (1941). *The Physics of Wind Blown Sand and Desert Dunes* London Methuen.
- Melo, H. P., Parteli, E. J., Andrade Jr, J. S., & Herrmann, H. J. (2012). Linear stability analysis of transverse dunes. *Physica A: Statistical Mechanics and its Applications*, 391(20), 4606-4614.
- Shehata, W., Bader, T., Irtem, O., Ali, A., Abdallah, M., & Aftab, S. (1992). Rate and mode of barchan dunes advance in the central part of the Jafurah sand sea. *Journal of arid environments*, 23(1), 1-17.
- Momiji, H., & Warren, A. (2000). Relations of sand trapping efficiency and migration speed of transverse dunes to wind velocity. *Earth Surface Processes and Landforms: The Journal of the British Geomorphological Research Group*, 25(10), 1069-1084.
- Andreotti, B., Claudin, P., & Douady, S. (2002). Selection of dune shapes and velocities Part 1: Dynamics of sand, wind and barchans. *The European Physical Journal B-Condensed Matter and Complex Systems*, 28, 321-339.
- Beelen, D. (2021). *The Sedimentology of Bottom Current Processes and Their Bedforms* (Doctoral dissertation, Colorado School of Mines).
- Eastwood, E. N., Kocurek, G., Mohrig, D., & Swanson, T. (2012). Methodology for reconstructing wind direction, wind speed and duration of wind events from aeolian cross-strata. *Journal of Geophysical Research: Earth Surface*, 117(F3).
- Jerolmack, D. J., Mohrig, D., Grotzinger, J. P., Fike, D. A., & Watters, W. A. (2006). Spatial grain size sorting in eolian ripples and estimation of wind conditions on planetary surfaces: Application to Meridiani Planum, Mars. *Journal of Geophysical Research: Planets*, 111(E12).
- Jackson, D. W., Bourke, M. C., & Smyth, T. A. (2015). The dune effect on sand-transporting winds on Mars. *Nature Communications*, 6(1), 8796.
- Long, J. T., & Sharp, R. P. (1964). Barchan-dune movement in imperial valley, California. *Geological Society of America Bulletin*, 75(2), 149-156.
- Haynes Jr, C. V. (1989). Bagnold's barchan: a 57-yr record of dune movement in the eastern Sahara and implications for dune origin and paleoclimate since Neolithic times. *Quaternary Research*, 32(2), 153-167.
- Sauermann, G., Rognon, P., Poliakov, A., & Herrmann, H. J. (2000). The shape of the barchan dunes of Southern Morocco. *Geomorphology*, 36(1-2), 47-62.

- Elbelrhiti, H., Andreotti, B., & Claudin, P. (2008). Barchan dune corridors: field characterization and investigation of control parameters. *Journal of Geophysical Research: Earth Surface*, 113(F2).
- Kennedy, J. F. (1969). The formation of sediment ripples, dunes, and antidunes. *Annual review of fluid mechanics*, 1(1), 147-168.
- Baddock, M. C., Nield, J. M., & Wiggs, G. F. (2018). Early-stage aeolian protodunes: Bedform development and sand transport dynamics. *Earth Surface Processes and Landforms*, 43(1), 339-346.
- Qian, G., Yang, Z., Tian, M., Dong, Z., Liang, A., & Xing, X. (2021). From dome dune to barchan dune: Airflow structure changes measured with particle image velocimetry in a wind tunnel. *Geomorphology*, 382, 107681.
- Sutton, S. L. F., McKenna Neuman, C., & Nickling, W. (2013). Avalanche grainflow on a simulated aeolian dune. *Journal of Geophysical Research: Earth Surface*, 118(3), 1767-1776.
- Elbelrhiti, H. (2012). Initiation and early development of barchan dunes: A case study of the Moroccan Atlantic Sahara desert. *Geomorphology*, 138(1), 181-188.
- Pye, K., & Tsoar, H. (2008). *Aeolian sand and sand dunes*. Springer Science & Business Media.
- Kok, J. F., Parteli, E. J., Michaels, T. I., & Karam, D. B. (2012). The physics of wind-blown sand and dust. *Reports on progress in Physics*, 75(10), 106901.
- Valance, A., Rasmussen, K. R., El Moctar, A. O., & Dupont, P. (2015). The physics of aeolian sand transport. *Comptes Rendus Physique*, 16(1), 105-117.
- Durán, O., Andreotti, B., & Claudin, P. (2012). Numerical simulation of turbulent sediment transport, from bed load to saltation. *Physics of Fluids*, 24(10).
- Manyonge, A. W., Ochieng, R. M., Onyango, F. N., & Shichikha, J. M. (2012). Mathematical modelling of wind turbine in a wind energy conversion system: Power coefficient analysis.
- Hersen, P. (2004). On the crescentic shape of barchan dunes. *The European Physical Journal B-Condensed Matter and Complex Systems*, 37, 507-514.
- Durán, O., Parteli, E. J., & Herrmann, H. J. (2010). A continuous model for sand dunes: Review, new developments and application to barchan dunes and barchan dune fields. *Earth Surface Processes and Landforms*, 35(13), 1591-1600.
- Dong, Z., Liu, X., Wang, H., & Wang, X. (2003). Aeolian sand transport: a wind tunnel model. *Sedimentary Geology*, 161(1-2), 71-83.
- Sørensen, M. (2004). On the rate of aeolian sand transport. *Geomorphology*, 59(1-4), 53-62.
- Ungar, J. E., & Haff, P. K. (1987). Steady state saltation in air. *Sedimentology*, 34(2), 289-299.
- Andreotti, B. (2004). A two-species model of aeolian sand transport. *Journal of Fluid Mechanics*, 510, 47-70.

- Martin, R. L., & Kok, J. F. (2017). Wind-invariant saltation heights imply linear scaling of aeolian saltation flux with shear stress. *Science advances*, 3(6), e1602569.
- Michel, S., Avouac, J. P., Ayoub, F., Ewing, R. C., Vriend, N., & Heggy, E. (2018). Comparing dune migration measured from remote sensing with sand flux prediction based on weather data and model, a test case in Qatar. *Earth and Planetary Science Letters*, 497, 12-21.
- Baird, T., Bristow, C. S., & Vermeesch, P. (2019). Measuring sand dune migration rates with COSI-Corr and Landsat: Opportunities and challenges. *Remote Sensing*, 11(20), 2423.
- Zheng, Z., Du, S., Taubenböck, H., & Zhang, X. (2022). Remote sensing techniques in the investigation of aeolian sand dunes: A review of recent advances. *Remote Sensing of Environment*, 271, 112913.
- Bristow, C. S. (2019). Bounding surfaces in a barchan dune: Annual cycles of deposition? Seasonality or erosion by superimposed bedforms?. *Remote Sensing*, 11(8), 965.
- Reitz, M. D., Jerolmack, D. J., Ewing, R. C., & Martin, R. L. (2010). Barchan-parabolic dune pattern transition from vegetation stability threshold. *Geophysical Research Letters*, 37(19).
- Barchyn, T. E., & Hugenholtz, C. H. (2012). A process-based hypothesis for the barchan–parabolic transformation and implications for dune activity modelling. *Earth Surface Processes and Landforms*, 37(13), 1456-1462.
- Wiggs, G. F., Livingstone, I., & Warren, A. (1996). The role of streamline curvature in sand dune dynamics: evidence from field and wind tunnel measurements. *Geomorphology*, 17(1-3), 29-46.
- Ewing, Kocurek, Jerolmack, Bustos, 2012, Constructing the Dune-Field Pattern at White Sands National Monument. White Sands Science Symposium, Research brief.
- Chojnacki, M., Banks, M. E., Fenton, L. K., & Urso, A. C. (2019). Boundary condition controls on the high-sand-flux regions of Mars. *Geology*, 47(5), 427-430.
- Hersen, P., Douady, S., & Andreotti, B. (2002). Relevant length scale of barchan dunes. *Physical Review Letters*, 89(26), 264301.
- Lonsdale, P., & Malfait, B. (1974). Abyssal dunes of foraminiferal sand on the Carnegie Ridge. *Geological Society of America Bulletin*, 85(11), 1697-1712.
- Southard, J. B. (1991). Experimental determination of bed-form stability. *Annual Review of Earth and Planetary Sciences*, 19(1), 423-455.
- Pähtz, T., & Durán, O. (2017). Fluid forces or impacts: What governs the entrainment of soil particles in sediment transport mediated by a Newtonian fluid?. *Physical Review Fluids*, 2(7), 074303.

SUPPLEMENTARY INFORMATION

S1: Dunefield measurements

S2: Surface areas covered

S3: Parabolic dunes

S4: Migration rate prediction

S5: Linear Regression

S6: Whitesands

S7: Normality test